JOINT EUROPEAN TORUS

JET–P(90)32

M.F.F. Marcus, D. Campbell, E. Joffrin, F.B. Marcus, G. Sadler, P. Smeulders,
K. Thomsen and JET Team

Fishbone Activity in JET

Fishbone Activity in JET

M.F.F. Marcus[1], D. Campbell, E. Joffrin, F.B. Marcus, G. Sadler, P. Smeulders, K. Thomsen and JET Team*

JET-Joint Undertaking, Culham Science Centre, OX14 3DB, Abingdon, UK

[1]Laboratorio Nacional de Engenharia e Tecnologia Industrial, Sacavem, Portugal
** See Appendix 1*

Preprint of Paper to be submitted for publication in
Nuclear Fusion

FISHBONE ACTIVITY IN JET

M.F.F.Nave*, D.Campbell, E.Joffrin,
F.B.Marcus, G.Sadler, P.Smeulders, K.Thomsen

JET Joint Undertaking, Abingdon, Oxon, U.K.
*Laboratorio Nacional de Engenharia e Tecnologia Industrial, Sacavem, Portugal.

Abstract

During auxiliary heating experiments in JET, periodic bursts of oscillations resembling 'fishbones' are observed in the signals of several diagnostics. Here the characteristics of these bursts are described and the regime over which they occur is analysed. In addition, the evidence for their interaction with high energy particles is considered and discussed in the light of the theoretical models of the instability which is believed to be responsible for the bursts.

1 - Introduction

Amongst the variety of MHD activity observed in JET during auxiliary heating experiments, periodic bursts of oscillations detected by several diagnostics show signatures similar to the fishbone instabilities observed in PDX /1-3/. In JET, two methods of auxiliary heating are employed:

(co-directional) neutral beam injection (NBI), with up to 21MW of 80keV deuterons, and ion cyclotron resonance heating (ICRH) using mainly fundamental heating of a minority species (H or ^{3}He) at powers up to 18MW. Both types of heating produce fishbone-like bursts /4/. We believe that this is the first observation of such bursts in radio-frequency heated plasmas.

The term 'fishbone' was first applied to describe the characteristic signature of short bursts of mhd oscillations observed in the diagnostic signals of high-β PDX discharges, which were heated with nearly perpendicular NBI /1-3/. Synchronous bursts were apparent in several signals, in particular soft X-ray emission (SXR) and magnetic pick-up coils. The bursts were superimposed on sawteeth and had a duration much sorter than the sawtooth period. The main component of the oscillations was identified as having poloidal and toroidal mode numbers m=n=1 in the plasma centre. However, the frequency of the mode was found to be significantly higher than that of the normal m=1 precursor to sawteeth, which had a frequency close to that of the bulk ion rotation frequency.

One of the most significant aspects of the activity was the observation of a sharp drop in neutron emission, corresponding to a loss of as much as one third of the beam injected ions, correlated with each burst. High time resolution measurements of fast ion losses using a neutral particle analyzer confirmed a substancial loss of fast particles at each burst.

This correlation stimulated an analysis of the influence of kinetic effects on the stability of the m=1 mode /5,6/. Briefly, although there are differences between the two principal theories, it was proposed that a population of energetic trapped particles could be responsible for

destabilizing such a mode. The m=n=1 oscillations were predicted to occur as a result of a resonance between the m=1 mode and energetic trapped ions within the q=1 surface. In addition, the characteristic growth and decay of the bursts was explained by a self-regulating mechanism in which the mhd mode scattered the fast particles required to drive the instability. Near-perpendicular NBI was thought to be essential to the generation of this instability as the proposed mechanism required a significant fraction of the beam ions to be injected into trapped orbits /5/.

Subsequently, observation of similar bursts of mhd ativity were reported from other tokamaks /7-12/ heated with either near-perpendicular or near-parallel NBI. In general, the bursts occurred in high-β discharges. In some cases /10,11/, a continuous m=1 mode was observed under similar conditions to those required for fishbone activity. In ASDEX, fishbones were observed in H-mode discharges in the absence of sawteeth /11/.

These observations have blurred the identity of fishbones. Strictly speaking, the term could be restricted to phenomena where a clear interaction with a fast particle population is observed. However, the term has come to be applied to all cases in which an m=n=1 mode exhibits the characteristic envelope of the type originally observed in PDX. The extension of the usage to cases where a continuous m=n=1 mode occurs is more problematic, but as we shall show here, the two types of activity are observed under identical conditions and the nature of the distinction between the two is not always clear.

The remainder of this paper is concerned with an analysis of m=n=1 activity observed during additional heating (NBI and ICRH) experiments in JET. We describe the characteristics of the mhd oscillations, discuss the

conditions under which they are observed and consider the evidence for their interaction with the energetic ion population.

2 - Observations

a) Characteristics

Repetitive bursts of coherent oscillations in the signals of the electron cyclotron emission (ECE), soft X-rays (SXR) and magnetics diagnostics are commonly observed in JET discharges with auxiliary heating. The bursts last for a few milliseconds and have a repetition time of typically ≃10-20ms, although occasionally longer repetition times of 40ms were observed. They are usually superimposed on sawtooth oscillations, however in a few cases they have also been observed during sawteeth-free periods /13/. Under some conditions continuous MHD oscillations are observed instead. Figure 1 shows the ECE signals for a discharge with ICRH in which both bursts and continuous oscillations where observed. The bursts are associated with small drops in the central temperature resembling partial sawteeth. The continuous oscillations sometimes cause large deformations of the sawtooth shape, clearly decreasing the ramp-up rate of the central temperature.

Magnetic mode analysis both in ICRH and NBI discharges reveals an n=1 toroidal component with frequencies typically in the range 5-10 kHz. There are however exceptions with very low frequencies of ≃ 1kHz observed in ICRH discharges, as in the example show in Figure 1, and frequencies as high as 20kHz in NBI discharges. Frequencies up to 50kHZ can be measured with the magnetic diagnostics and 100kHZ with SXR diagnostics. Within this range, higher frequency precursors, as observed in PDX /2,3/, have not

been seen in JET.

The poloidal structure cannot be precisely determined from the magnetic signals, probably due to a strong coupling between m=1 and m=2 components which perturbs the phase. It can however be determined from tomographic reconstruction of soft X-rays and from the projection of ECE signals in the poloidal plane. These methods show an odd mode near the sawtooth inversion radius, which is likely to be a m=1 perturbation. Although the m=1 is dominant, other, higher m number components, m=2 and m=3, are also observed outside the sawtooth inversion radius. The ECE signals shown in Figure 1, are out of phase on each side of the centre for both the bursts and the continuous oscillations, indicating a m=1. Figure 2 shows the soft X-ray tomographic reconstructions for a burst. An m=1 perturbation resembling an island is clearly seen around the q=1 radius, which is obtained by the calculation of the magnetic equilibrium /14/. A similar picture is obtained during the continuous oscillations. The island widths of around 10cm obtained from the SXR data are comparable to flattenings around the q=1 radius observed in the LIDAR temperature profiles /15/. So it becomes clear that the fishbones observed in JET have the same structure as an m=1, n=1 resistive kink mode.

When the frequency of the bursts is close to that of the plasma rotation, the distinction between this type of activity and sawtooth-related oscillations becomes less clear. In particular, the distinction becomes difficult during JET high-β operation, as will be discussed later. However, in many discharges the frequency of the bursts is higher than the frequency of oscillations associated with sawtooth activity. This is illustrated in Figure 3, where the magnetic signals detected during an ICRH heated discharge show the slow oscillations appearing after a

sawtooth collapse preceeded and followed by several higher frequency bursts. This figure also shows that the fishbone oscillations rotate in the direction of the plasma current, which is also equivalent to a poloidal rotation in the direction of the ion diamagnetic drift.

In JET the oscillations around the sawtooth collapse, for either the partial or the full sawtooth, are observed to rotate with the same frequency as the plasma /16/, and therefore the example in Figure 3 shows clearly that the fishbone bursts are an independent phenomena with a frequency of their own and are distinct from the oscillations related to sawtooth collapses. For a more detailed comparison between the two phenomena, Figure 4 shows the soft X-ray emission at different radial positions for the sawtooth postcursor and for one of the higher frequency bursts. The sawtooth postcursor is an event of larger amplitude with a heat pulse visible at the outer positions. The fishbone burst is visible only inside the sawtooth inversion radius. The similarities are that both the postcursor and the fishbones are m=1, n=1 modes (although the fishbone has a broader mode spectrum) and both have their maximum amplitude around the sawtooth inversion radius. Fishbone amplitudes obtained from magnetic signals are low, typically the poloidal field fluctuations on the mid-plane on the external side of the plasma are $b_p/B_p \sim 10^{-4}$-$3x10^{-4}$.

Both bursts and continuous oscillations may have frequencies up to 10 times the bulk plasma rotation frequency. At JET two techniques are used to determine the plasma rotation: spectroscopy of Doppler-shifted emission lines of heavy impurities in the X-ray domain; and charge exchange of light impurities with NBI neutrals at the centre of the plasma. Figure 5 shows the frequency spectra of a sequence of fishbone bursts observed in a NBI heated discharge, with the peak frequency in each spectrum 4kHZ higher

than the central plasma rotation. In this example, the increase in frequency from 6.5KHz to 10KHz between the first and the last burst reflects the same increase in the central plasma rotation, showing that the fishbone frequency has remained the same in the plasma rest frame. The increase in the maximum amplitude for each burst is also apparent. Moreover, the figure shows the development of a continuous mode after the amplitude of the last burst has saturated to a constant level.

The frequency slows down during a burst and has been observed to decrease by up to a quarter of its initial value. It is found that the slowing down of the frequency during a burst is faster for lower values of the edge safety factor. A typical burst with a plot of the frequency evolution is shown in figure 6. The spectral analysis normally reveals lower frequency n=1 modes rotating with the bulk plasma. These low frequency oscillations are clearly seen in between the high frequency bursts and also in the form of a modulation in the bursts' envelopes. The frequency plot, in figure 6, show the evolution of the frequency of the fast oscillation during a burst, and for comparison, it also shows the frequency of the slower oscillation. (The relationship of fishbones to the slower oscillations and other mhd activity, which are sometimes seen overlapping with them will be discussed later.) The burst frequency decreases rapidly while the amplitude is rising, then locks to a value still higher than the plasma rotation frequency. After the burst the frequency again increases to the initial higher value.

b) Conditions for the observation of 'fishbones'

Fishbones are observed over a wide range of the JET operating space with auxiliary heating. A plot of the observations in a Hugill diagram, in

figure 7, shows that they occur in a broad region, being common at low as well as high values of q_a. One notices, however an absence of points for high values of the Murakami parameter. In fact, neither bursts or continuous oscillations were observed in discharges operated close to the density limit with either NBI or ICRH heating.

Apart from the absence in high densities, JET fishbones occur in both the L and H confinement regimes and have been observed over the whole range of poloidal and toroidal β values. JET has been operated with values of $\beta_p \leq 1.0$ and $\beta_T \leq 5.5\%$. Figure 8a shows observations of bursts in a diagram of β_p versus the total input power. Figure 8b shows the same observations in a diagram of β_N versus the total input power, where β_N is the toroidal β normalised to the Troyon limit ($\beta_{Troyon} = 2.8\ I_p(MA)/(B_\phi(T)\ a(m))$ /16/. While in other experiments fishbones are observed above very clear β thresholds, at JET there seems to be no lower β limit for their appearance. The apparent lower limit in $\beta_p \sim 0.1 \pm 0.4$ (for an assumed error in the measured diamagnetic flux of 20mVs) reflects only a lower limit on the confinement time.

The continuous oscillations do not seem to occur for any particular values of the input power, or of any other parameters. However, in ICRH heated discharges their appearence seems to be affected by the choice of minority gas, since they are seen more often with ^{3}He minority heating.

c) Fishbone activity during high β operation

JET has been mostly operated at values of beta toroidal well below the Troyon limit, i.e. with $\beta_N < 0.7$. For higher values some of the fishbone-like characteristics described above are modified.

Toroidal beta values close to the Troyon limit were obtained in discharges with B_ϕ<1.2T and I_p=2MA. A complex variety of mhd activity is observed in that regime and it will be described elsewhere /18/. Here we concentrate on the fishbone activity. As mentioned previously fishbones in JET are not specifically a high β phenomena, however in this regime they have larger amplitudes and seem to play an important role in limiting the toroidal β values.

Figure 9, shows a discharge where during the saturation of β_N fishbone activity occuring alongside ELMS /19/ is observed. The larger amplitude sawtooth event which finally reduces β_N, bears a closer similarity to a fishbone than was observed in low β regimes. The differences and similarities are illustrated in Figure 10, which shows, for another discharge with β_N~1, the soft X-rays signals for a fishbone burst, i.e. for a burst before a β_N crash, and for a sawtooth responsible for a β_N relaxation. The sawtooth has a very fast heat-wave propagating outwards (similar to but one order of magnitude faster than the one normally observed in low β sawtooth collapses), which is not observed with the fishbone. The frequency of the oscillations around the two events are comparable. Charge exchange measurements available at different radii show that both have the frequency of rotation of the plasma at the q=1 surface. Thus the higher frequency which clearly distinguished the fishbone from other m=1, n=1 oscillations is no longer observed.

In the high β regime fishbones have larger amplitudes everywhere in the plasma as shown in Figure 10. When compared to the low-β fishbones, as in in Fig.4 where β_N=0.18, the amplitude at the sawtooth inversion radius is 10 times larger. It is also clear that, at high-β, the mode activity is no longer localised around the sawtooth inversion radius but extends to

larger plasma minor radii with a large asymmetry in the mid-plane between the inner and the outer major radius. Figure 10 shows that the oscillations are clearly visible up to the outside edge of the plasma, indicating a ballooning effect. Amplitudes obtained from magnetic measurements, taken outside the plasma, are enhanced by the ballooning effect and therefore are no longer a good indication of the fishbone amplitude. A lower limit of $b_p/B_p \sim 3 \times 10^{-3}$ is obtained from the magnetic signals at the outer midplane for fishbones occuring at β_N=0.7 (for higher β_N the magnetic signals are saturated).

d) Interaction with the fast particle population

The MHD characteristics of fishbones in JET exhibit similarities with those observed in PDX discharges, but the associated fast ion losses observed so far seem to be significantly weaker. Five diagnostics are used to observe the time dependence of the fast ion population: charge exchange neutral particle detectors (NPA); neutron-detecting fission chambers; a neutron profile monitor; a NaI(Tl)-scintillator which is sensitive to fast neutrons and neutron capture γ-rays, and hence to the total neutron emission; and a covered soft X-ray Si-diode, which is sensitive to neutrons and hard X-rays. However, all of these diagnostics have, at present, some limitations for the observation of fishbones.

The NPA shows fast ion losses following a sawtooth collapse. However, no clear evidence is seen of losses during the fishbones. This is possibly due to a limited time resolution.

During fishbone events, the changes in the neutron emission are within the 5-10% noise limit of the fission chambers if operated at the required fast

time scale. However, the neutron-induced signals in the NaI (Tl)-scintillator, when available on a fast time scale, show sudden drops during fishbone bursts. This is shown in Figure 11 for a discharge with β_N=0.7, for which changes in the total global emission of about 9% were estimated. The covered soft X-ray Si-diode has also observed fishbone events during high β operation. Figure 12 shows observations at β_N=1, where an estimated drop of 19% in the neutron rate is obtained. However, even for the large amplitude fishbones seen in high-β discharges, the changes in the neutron rate are not as large as the ones observed during sawtooth collapses. This is also illustrated in Figure 12, where the drop in the Si-diode signal observed during the sawtooth crash is twice that observed during the fishbone.

The lower rate of losses due to fishbones in JET, compared to PDX, may be due to the large size of the JET plasma which leads to a better confinement of the fast particles. In general, sawtooth collapses at JET are observed both with the neutron fission chambers and the neutron profile monitor. However, due to a redistribution of the fast particles, changes in the global emission may be small and in some cases are not even observed /20/. Similarly, the small changes in the global emission observed during fishbone events could also be due to a redistribution of fast ions. An alternative explanation might be the low amplitude of the poloidal field fluctuation associated with the bursts. The highest amplitudes observed in JET high-β regimes, although just over the PDX threshhold for observation of loss of energetic ions /3/, are still one order of magnitude smaller than the largest amplitude events observed in PDX.

As a further test on how the fishbone instability is affected by the

presence of fast particles, its occurrence was studied as a function of the electron density. In discharges with an electron density close to the density limit, i.e. with a very short slowing down time which implies a low energy content in the fast particles, m=1, n=1 oscillations with frequencies higher than the frequency of rotation of the plasma were not observed either in the magnetics, ECE or SXR signals.

e) Effect on plasma confinement

For the typical JET fishbone, observed at low-β_N, no significant effect on plasma confinement has been observed. Figure 13 shows no systematic difference between the energy confinement times of fishbones-like events and quiet sawteeth-free periods (H-modes have being excluded from the figure). At high-β_N, the particle losses per fishbone event are still smaller than those due to sawtooth collapses, as described above. However, the associated loss of energy could be more significant on account of their higher repetition rate.

In high current ICRH discharges the instabilities seem to be affected by the choice of minority gas. Although fishbone activity is found in discharges heated with either ^{3}He or H minority gas, the relative amplitude of the oscillations seen in the ECE signals is twice as large in the ^{3}He case. Also with ^{3}He, continuous oscillations are observed more frequently than bursts (see Figure 14). The discharges with ^{3}He minority gas are found to have a confinement about 30% lower than that predicted by the Goldston L- mode scaling /21/. Recent studies /22/ have shown a correlation between decreased confinement and large mhd activity observed in JET. However, further studies are required to verify quantitatively the apparent correlation between the poor confinement and the enhanced

fishbone activity observed in the ICRH discharges heated with ^{3}He minority gas.

f) Fishbones and other mhd activity

Fishbones in JET normally occur alongside other mhd activity. A typical spectrum from magnetic signals reveals slower n=1 oscillations, some rotating in the same direction as the fishbones, others rotating in the opposite direction. During the H-mode regime fishbone bursts and ELMs are seen occurring independently of each other (as illustrated in Fig.9), as may be expected because of their different spatial location. Higher n numbers are also observed during high-β operation /18/.

From the point of view of the theory it is interesting to look at the relationship between fishbones and sawteeth. As mentioned before, the fishbone and the sawtooth collapse can often be distinguished from one another in low β regimes, however the differences become less clear for values of β close to the Troyon limit. The sawtooth collapse often occurs during a fishbone burst, possibly because of the high frequency of occurrence of fishbones. It should also be noticed that at JET fishbones have been observed during sawtooth-free regimes, although this is a much rarer event.

(i) Sawtooth regimes

Fishbone activity is present during the whole of the sawtooth ramp. This is quite clear in Fig. 3 which shows that the bursts reappear soon after the sawtooth collapse (in this example it took 30ms), even before the sawtooth postcursor has died away. If fishbones are present, the sawtooth crash occurs very often during these oscillations, however it does not

seem to be triggered by them. If a sawtooth collapse occurs during a fishbone (burst or continuous mode), the fast m=1 mode does not survive the collapse.

The frequency spectra in general reveals two distinct frequencies, both corresponding to m=1,n=1 perturbations. In some discharges the two frequencies remain visible during the whole of the sawtooth ramp.

In Figure 15 we look in more detail at the example shown in Figure 6. It shows the magnetic signals observed during a combined NBI/ICRH heating discharge. It displays two oscillations during the whole of the sawtooth ramp, a low frequency oscillation of 1.2KHz comparable to the central frequency of rotation of the plasma and a higher frequency oscillation of 8KHz. The amplitude of the slow oscillation remains constant, while the amplitude of the fast oscillation rises and decreases periodically giving rise to the fishbone bursts. During a burst the higher frequency slows down to 3kHz as shown in figure 6. The slow oscillation is unaffected by the burst and is observed as a modulation on the bursts envelop. Both oscillations show an n=1 toroidal component, and soft X-ray signals show that both have large m=1 components at the plasma centre. From soft X-ray signals it has been seen that the slow oscillation is not a satellite of a higher m oscillation.

The close-up of the sawtooth crash in the same figure, shows the fishbone burst cut short by the sawtooth collapse and a postcursor oscillation with a frequency close to the one of the preceeding slow oscillation which overlaps the burst. Since the instability causing the collapse grows on a time scale much shorter than any of the oscillations seen, it is not clear whether the slow oscillation could be responsible for it. In this

discharge all three oscillations, i.e. the sawtooth postcursor, the preceeding slow oscillation and the faster fishbone, rotate in the direction of the ion diamagnetic drift. Although, in discharges heated with ICRH only, as in the example in Figure 4, the sawtooth poscursor may rotate in the opposite direction to the fishbone.

(ii) Sawtooth free-periods

In most cases, both the bursts and the continuous oscillations are seen superimposed on the sawtooth oscillations. There are however a few observations of bursts during sawtooth-free periods. JET sawteeth-free periods occur during ICRH heated discharges and less often during NBI and combined heating discharges /13/. Fishbones were very occasionally observed in both types of sawtooth-free periods. Although MHD activity is more often seen during the rising phase of the sawtooth-free period, there were also examples of X-point discharges which showed fishbone bursts during the flat phase of sawtooth-free periods as illustrated in figure 16.

3 - Theoretical considerations

Theoretical models /5,6/ suggest that the fishbone instability is caused by the resonance between an m=1, n=1 mode and trapped energetic ions inside the q=1 surface. More recently it has also been suggested that fishbones and sawtooth supression in the presence of energetic ions may be intrinsically related, as both phenomena would be explained in terms of a single dispersion relation /23,24/. This dispersion relation, which includes the effects of the fast ions and of a finite Larmour radius, has

two roots, a slow mode with $\omega<\omega_i^*/2$, and a fast mode with $\omega>\omega_i^*/2$, where ω is the mode frequency in the plasma rest frame and ω_i^* is the ion diamagnetic frequency of the bulk plasma. The slow mode is the internal kink mode often suggested as a possible cause for the sawtooth instability /25/, while the fast mode is believed to be responsible for fishbones. The presence of energetic ions has opposite effects on the two modes. They may destabilize the fast mode, while damping the slow one. The pulsating behaviour of the fishbone is explained as follows. Initially, a mode-particle resonance occurs for ions with energies and magnetic moments such that their drift velocity equals the mode phase velocity. At a later time, scattering will reduce the number of resonanting particles within the resonant region, letting the resistivity take over and causing the damping of the mode /6,23/.

The fishbone frequency is predicted to range between the ion diamagnetic frequency, and the precession frequency of fast ions trapped inside the q=1 surface. Two distinct fishbone regimes have been indicated. These are characterised by different values of the beta poloidal of the bulk plasma, β_p^*, and the beta poloidal of the energetic ions, β_{ph}^*, both calculated at the q=1 surface. At the higher end of the spectrum, fishbones with frequencies of the order of the fast ion precession frequency occur for high values of β_{ph}^* /5/. Lower frequency fishbones with frequencies comparable to the ion diamagnetic frequency would occur for low values of β_{ph}^* and values of $\beta_p^*>\beta_{p,mhd}$ /6/, where $\beta_{p,mhd}$ is the ideal MHD threshold /26/. In both regimes, fishbones are unstable outside the stable domain associated with sawtooth supression.

Qualitatively, some of the JET observations of fishbones could be explained by these models. There are clearly two m=1, n=1 modes with

distinct frequencies, the fast one with frequencies up to 10 times the slower one. The fishbones rotate in the direction of the ion diamagnetic drift, as is also predicted by the models. When a sawtooth crash occurs during a fishbone, the large loss of fast ions caused by the collapse may stabilize the fishbone explaining why the fishbone is observed to be terminated by the sawtooth relaxation. It is, however, not clear whether the models could explain the observation of fishbones during the sawtooth-free periods, since this would require an overlapping between the regions for sawtooth stabilisation and for the existence of fishbones.

Detailed comparison between the theory and the experimental results is complex because of the difficulties associated with: the determination of the fast ion profile needed to calculate β_{ph}^{*} and the precession frequency of the fast ions; the uncertanty in the shape of the q profile inside of the q=1 surface needed to calculate $\beta_{p,mhd}$; the uncertainties in the plasma gradients at the q=1 surface needed to calculate the ion diamagnetic frequency. In addition, there is an uncertainty of ~ 1kHz in the central plasma rotation measurements, making it difficult to determine the mode frequency in the rest frame for some ICRH discharges.

The observed initial mode frequency in the plasma rest frame varies between the ion diamagnetic frequency for some ICRH discharges and the fast ion precession frequency, mostly for NBI discharges. Thus, in principle, the observed fishbones may fall in either predicted regime. One possible difficulty in explaining the observations in the low frequency regime could be the low values of β_p observed. However, the low-β_p discharges have also high values of the plasma current and consequently the q=1 surface occur at large radii (>0.4a). As the q=1 radius is increased $\beta_{p,mhd}$ decreases /26/, it is therefore possible that even in the

low-β_p regimes the condition $\beta_p^* > \beta_{p,mhd}$ is satisfied. A more detailed analysis clearly requires calculation of the threshold for ideal stability. In addition, for larger q=1 radii the stable domain shrinks considerably, which may account for the increasing difficulty in stabilising sawteeth and for the more likely occurrence of fishbones at high currents. Further assessment of the models, also with respect to sawtooth stabilisation, will be presented elsewhere.

The enhanced activity observed in ICRH discharges with ^{3}He minority gas, can also be qualitatively understood from the models. With ^{3}He minority the energy content of the fast ions inside the q=1 surface is lower than with H minority. The lower energy, means that more fast ions are available to resonate with the mhd mode. If we consider ^{3}He and the H cases where fishbones are observed in the low frequency regime, the smaller value of the fast ion precession frequency obtained for ^{3}He gives a larger growth rate /24/. One may therefore expect that the instability could grow to large amplitudes with ^{3}He. The models, being linear, will not, however, explain the mode saturation and the observation of continuous oscillations.

4 - Conclusions

Fishbones are a common feature of JET discharges with auxiliary heating. They are seen either as repetitive bursts, lasting a few milliseconds, or as continuous oscillations. They are observed both in neutral beam and ion cyclotron heated pulses, but their characteristics seem to be dependent on the heating system and plasma conditions used. They are observed during sawtooth and, occasionally, sawtooth-free regimes. Most JET discharges are

operated at low values of the normalized toroidal beta, below 70% of the Troyon limit, thus fishbones at JET are typically a low beta event. They are very common at low values of the edge safety factor q, and there seems to be no lower limit for their occurrence either in β_p or β_T.

In the low-β regimes, a high frequency, up to 10 times that of the central plasma rotation, clearly distinguishes the bursts and the continuous oscillations from other observed m=1, n=1 oscillations. For ICRH discharges, the instability seems to be affected by the choice of minority gas. For 5MA discharges, the amplitude of the oscillations observed is larger for ^{3}He than for H minority. Also for ^{3}He, the instability appears mostly in the form of continuous oscillations.

As both the toroidal and poloidal beta values are increased, larger amplitude oscillations are observed. For β_T approaching the Troyon limit, the amplitudes reach values comparable to the ones for which losses of fast ions became important in PDX. These large amplitude oscillations are seen during the saturation of β_T. Measurements available on a fast time scale indicate that the total neutron rate associated with the loss of fast particles may fall by 9-19% during a burst in the high β regime. The distinction between fishbone oscillations and the oscillations around a sawtooth become unclear in the high-β regime as both have the same frequency. A summary of the observed characteristics for either bursts or continuous oscillations is given in table I.

A preliminary comparison with the theoretical models shows that the observed frequency in the rest frame varies between the ion diamagnetic frequency and the fast ion precession frequency, thus both of the predicted fishbone regimes are possible in JET. A more detailed comparison

between predictions and observations should take into account the relationship between fishbones and other m=1, n=1 activity.

The distinct high frequency, plus some observed effect on the fast particle population, although smaller than in PDX, leads to the conclusion that the instabilities observed in JET are indeed similar to the PDX fishbones.

Table I

JET observed characteristics of fishbones	
burst duration	2-10ms
burst repetition time	10-20ms
mode analysis	m=1, n=1
typical frequencies	ν~6-10Khz
comparison with plasma bulk rotation	ν~1-10 ν_{rot}
mode rotates in the direction of the ion diamgnetic drift	
amplitude of the poloidal field fluctuation	$b_\theta/B_\theta \sim 10^{-4}-3\times10^{-3}$
maximum change in neutron rate	9-19% (for $\beta_N \geq 0.7$)

Acknowlegements

We are greatfull to many useful discussions with members of the JET team, and in particular we would like to thank Drs. F. Pegoraro, F. Porcelli, L. Eriksson and S. Corti.

References

/1/ Mcguire, K. et al.,Phys.Rev.Lett. 50,891 (1983)

/2/ Johnson, D.et al., plasma Phys. and Contr.Fus., vol.1,p.9 (1982)

/3/ Strachan, J. D. et al., Nuc. Fus.**25**, 863 (1985)

/4/ Nave, M.F.F.et al., in Contr. Fusion and Plasma Phys. (Proc. 16th EPS Conf., Venice), **13B**,part II,(1989) 505

/5/ Chen, L.,White, L. B., and Rosenbluth, M. N., Phys.Rev.Lett. **52**, 1122 (1984)

/6/ Coppi, B. and Porcelli, F, Phys.Rev.Lett. **57**, 2722 (1986)

/7/ Heidbrink, W. et al.,Phys.Rev.Lett 57,835 (1982)

/8/ Overskei, D. et al, in Heating in Toroidal Plasmas, ed. by H. Knoeptel and E.Sindoni (ENEA, Rome), vol.2,p.21 (1984)

/9/ Morris, A. et al.,Proc. 14th EPS (Madrid), vol.II,p.189 (1987)

/10/ Ishida, S. et al., in Recent Diagnostic Results of JT-60 Plasma, JAERI-Memo,62-224 (1987)

/11/ Kluber, O. et al., Proc. 13th EPS (Schliersee), (1986)

/12/ Heidbrink, W.W. and Sager, G., to appear in Nuc.Fus. (1990)

/13/ Campbell, D. J. et al.,Phys.Rev.Lett.**60**, 2148 (1988)

/14/ Lazzaro,E.,and Mantica,P., Plasma Phys. Contr.Fus.**30**, (1988) 1735

/15/ Nave, M. F. F., Lazzaro, E., Gowers, C., Hirsch, K., Nielsen, P. et al, in Contr. Fusion and Plasma Heating (Proc. 15th EPS Conf., Dubrovnik), **12B**, part I, (1989) 441

/16/ Stork, D., et al., Procc. 14th EPS Conference vol.1, p.306 (1987)

/17/ Troyon, F., Gruber, R. et al, Plasma Phys. Contr. Fusion **26** ,209 (1984)

/18/ Smeulders, P. et al, in preparation

/19/ Cripwell, P. et al, in Contr. Fusion and Plasma Phys. (Proc. 16th EPS Conf., Venice), **13B**,part I,(1989) 225

/20/ Marcus, F. et al., in Contr. Fusion and Plasma Phys. (Proc. 17th EPS Conf., Amsterdam) (1990)

/21/ The JET Team, Plasma Physics and Controlled Fusion **11**, 1467 (1988)

/22/ Snipes, J.A., Campbell, D.J., Hugon, M., Morgan, P., Stork, D. et

al., in Contr. Fusion and Plasma Heating (Proc. 15th EPS Conf., Dubrovnik), **12B**, part I, (1989) 346

/23/ Coppi, B.et al., Phys.Rev.Lett. **63**, 2733 (1989)

/24/ White, R. B. et al, Phys.Rev.Lett. **62**,539 (1989)

/25/ Coppi, B. et al., Sov.J.Plasma Phys.**2**, 533 (1976)

/26/ Bussac, M. N. et al., Phys.Rev.Lett **35**, 1638 (1975)

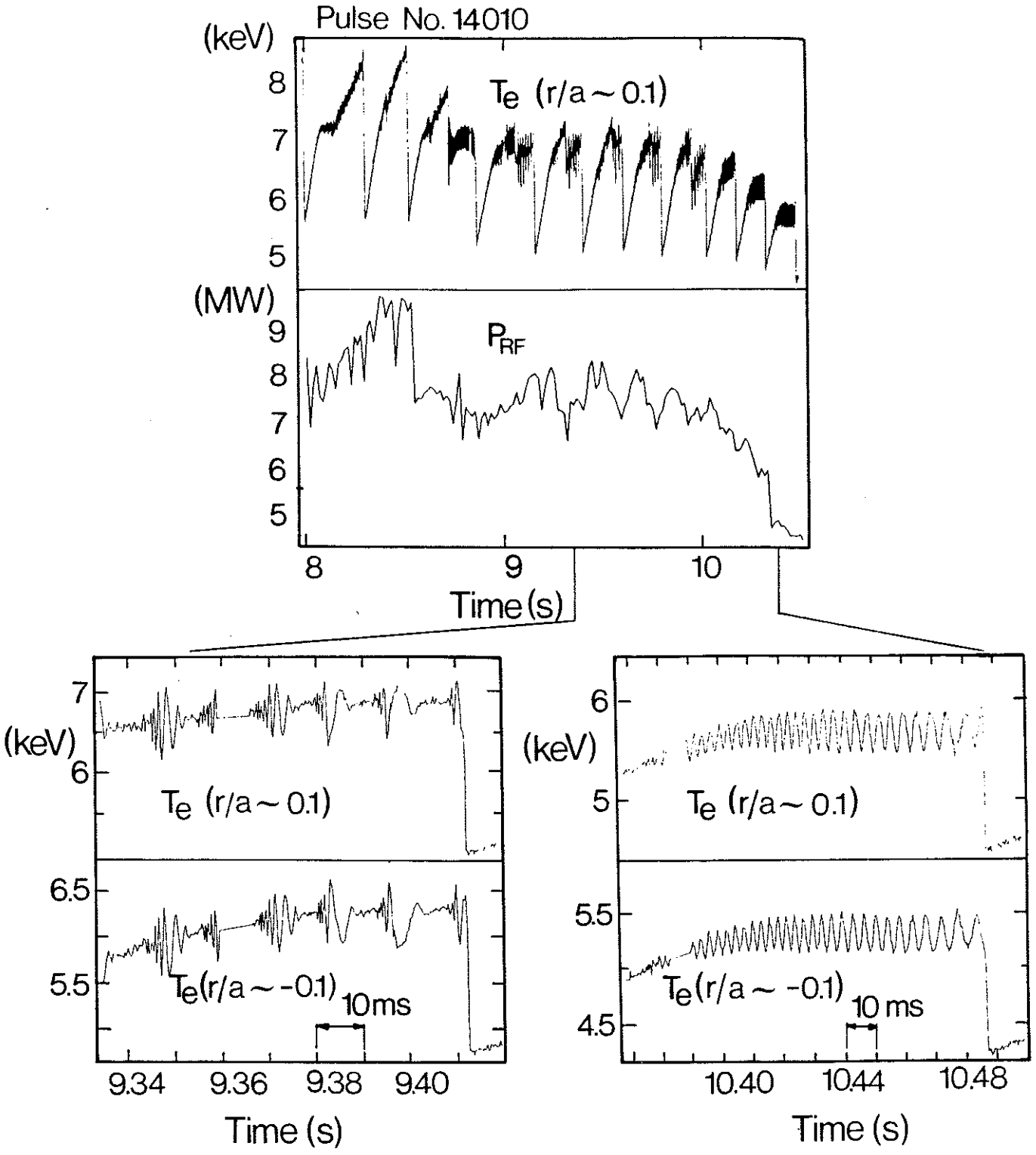

Figure 1 - Temperature and ICRH power versus time for an ICRH heated discharge showing both bursts and continuous oscillations. Both types of activity exhibit a phase inversion about the plasma centre' indicating an odd mode, where detailed analysis confirms that the mode has an m=1 component.

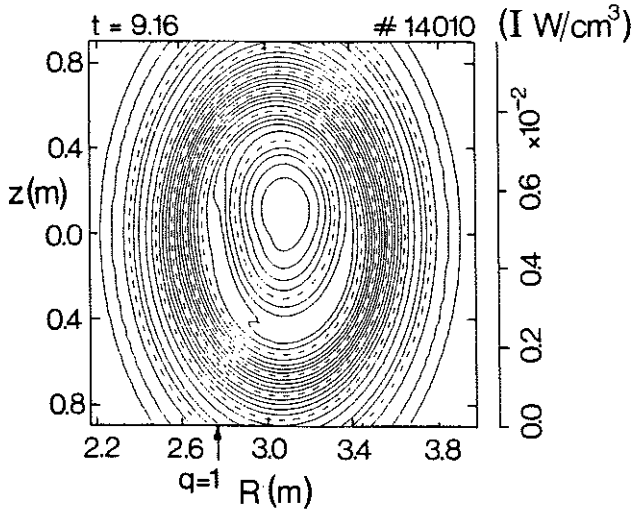

Figure 2 - Soft X-ray tomographic analysis for one of the bursts seen in the discharge shown in figure 1. The position of the q=1 surface, as determined from the magnetic equilibrium is indicated.

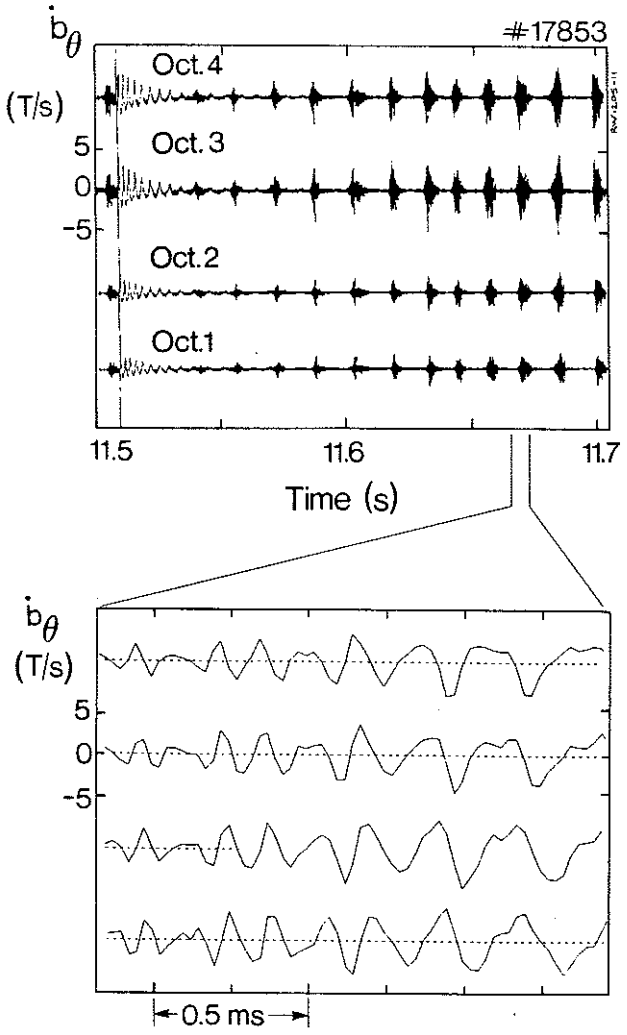

Figure 3 - Magnetic signals from pick-up coils at a fixed poloidal position (45° above the mid-plane on the lower field side) placed at different octants.

a) the oscillations of a sawtooth postcursor, preceeded and succeeded by several higher frequency fishbone bursts.

b) fishbone oscillations showing a phase shift which indicates rotaton in the direction of the plasma current.

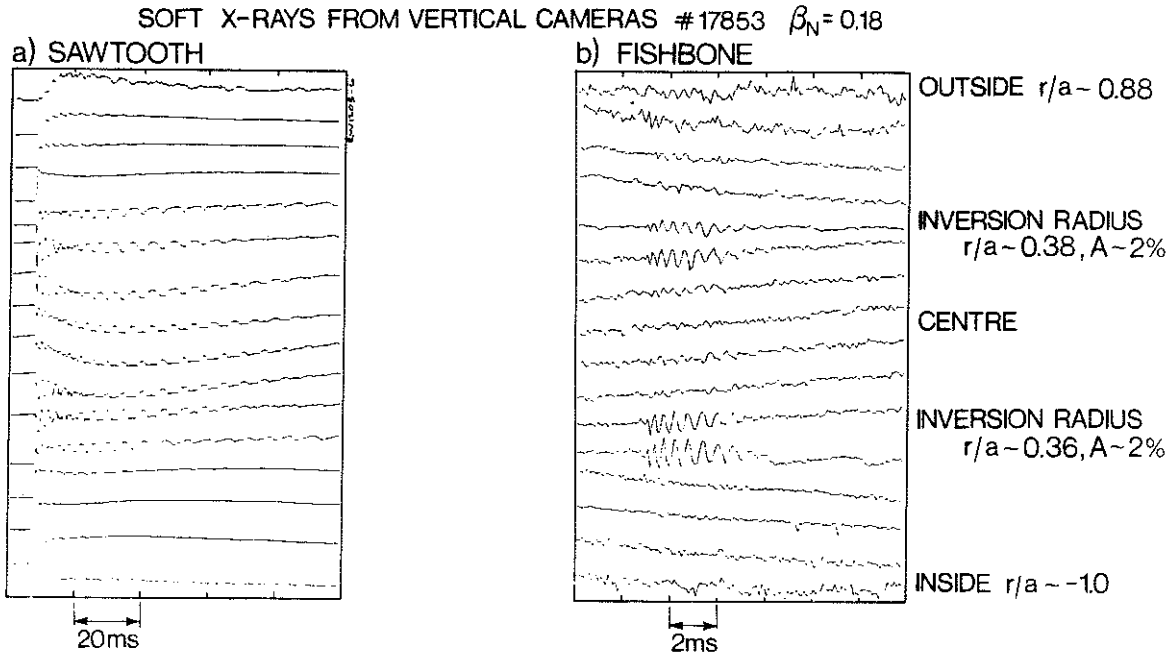

Figure 4 - Soft X-ray emission, at different radial positions on the mid-plane, for the sawtooth collapse, on the left, and a fishbone burst, on the right. $\tilde{A}$ is the relative amplitude at the position of the sawtooth inversion radius, where both phenomena have maximum amplitude.

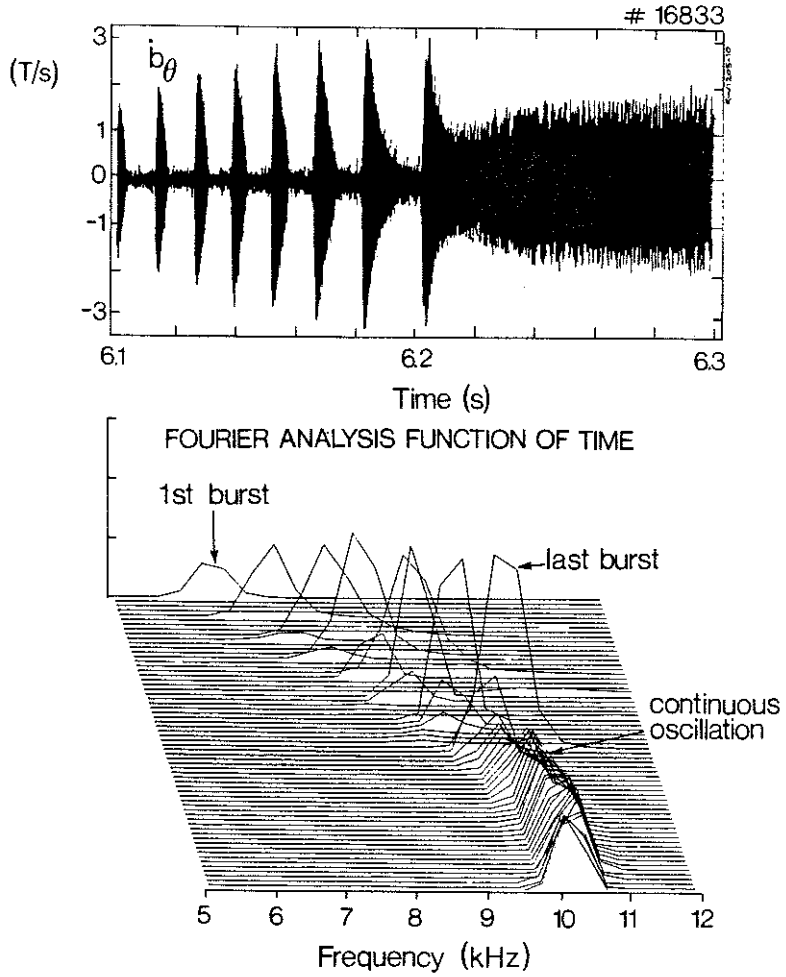

Figure 5 - (a) Magnetic signal (on the mid-plane on the lower field side) for a NBI discharge showing a continuous oscillation developing after a sequence of bursts.

(b) Power spectra of the signals in (a). The frequency increase reflects an increase in the plasma rotation.

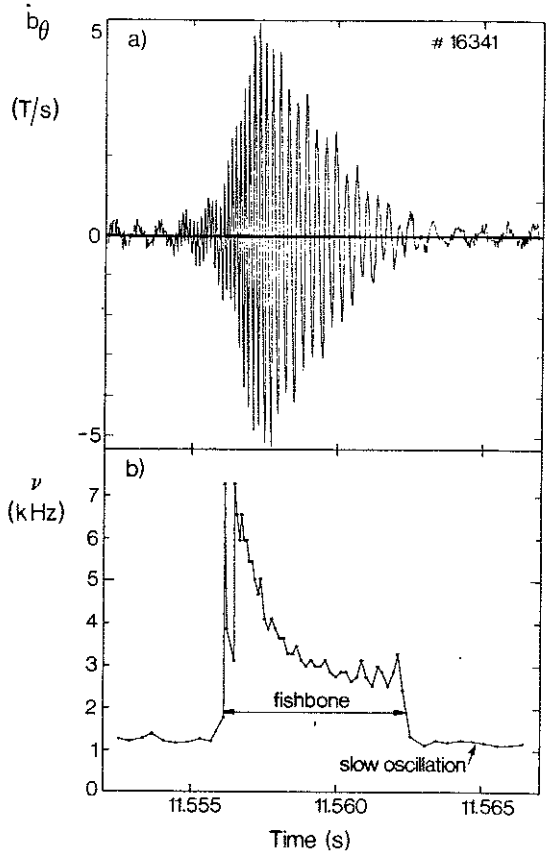

Figure 6 - (a) magnetic signal (n=1 combination measured at 45° above the mid-plane on the lower field side) for a typical burst observed during combined heating.

(b) Frequency evolution during the burst. For comparison the frequency of a slower oscillation, observed in this discharge both in between and overlapping the fishbone bursts, is also plotted. The slower oscillation has a frequency comparable to the central frequency of rotation of the bulk plasma.

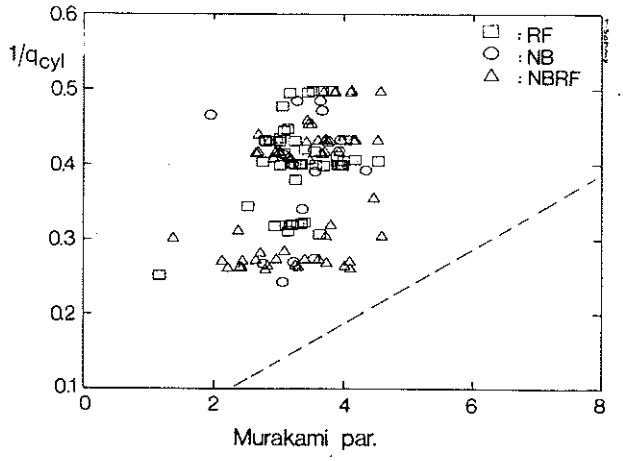

Figure 7 - Hugill Diagram for fishbone observations from a series of JET discharges. The line shows the density limity for that period of JET operation.

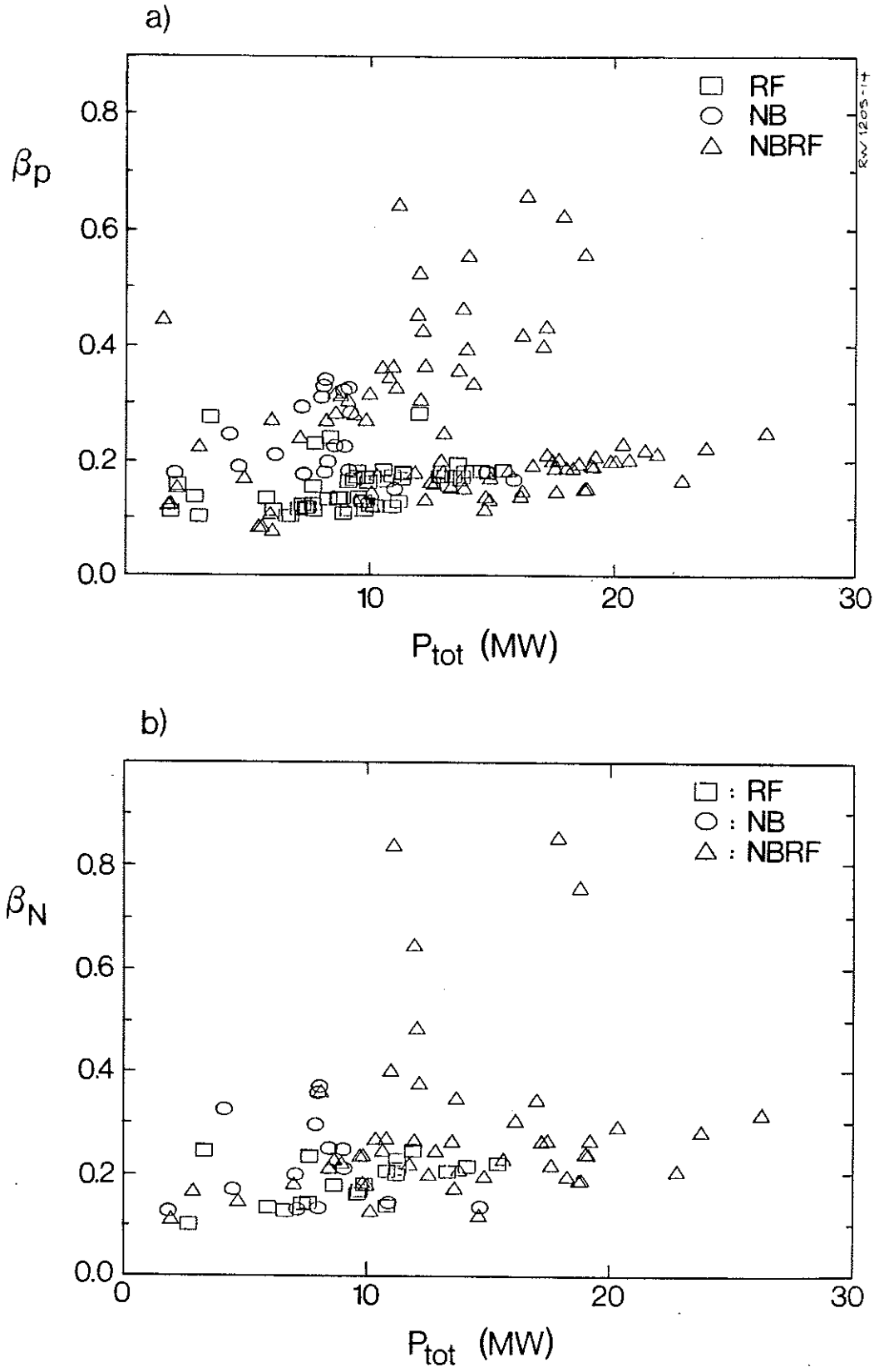

Figure 8 - (a) Fishbone observations in a diagram of β_p, the total diamagnetic poloidal beta, versus the total input power. The two branches reflect a difference in the total plasma current, i.e. most of the observations of $\beta_p < 0.25$ have $I_p > 4$MA.

(b) Fishbone observations plotted in a diagram of the normalized toroidal beta, $\beta_N = \beta_T / \beta_{Troyon}$, versus the total input power.

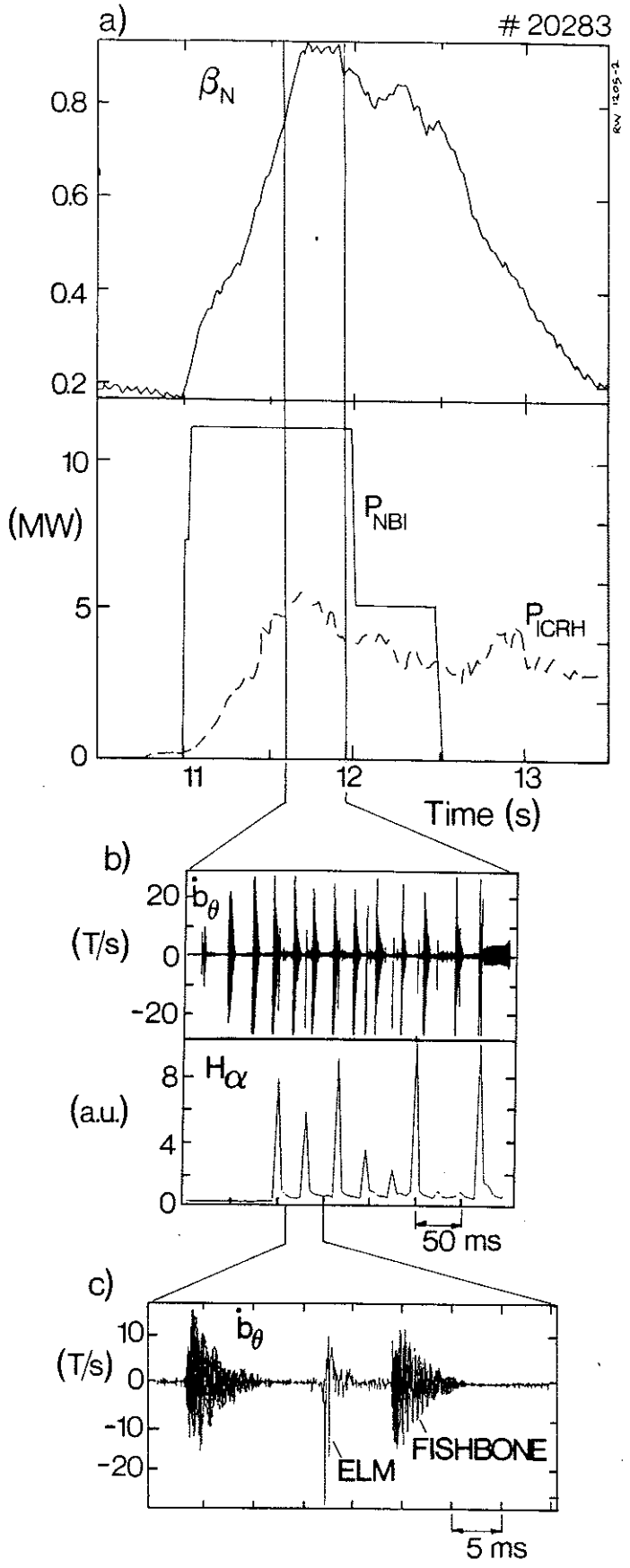

Figure 9 - (a) β_N, NBI power and ICRH power as a function of time.

(b)Magnetic signal (at 45° above the mid-plane on the lower field side) and H-α emission, measured at the X-point, versus time. The very rapid events seen in the magnetic signal and correlated to the H-α signal are elms.

c)A close-up of a magnetic signal measured near the X-point showing an elm between fishbone bursts.

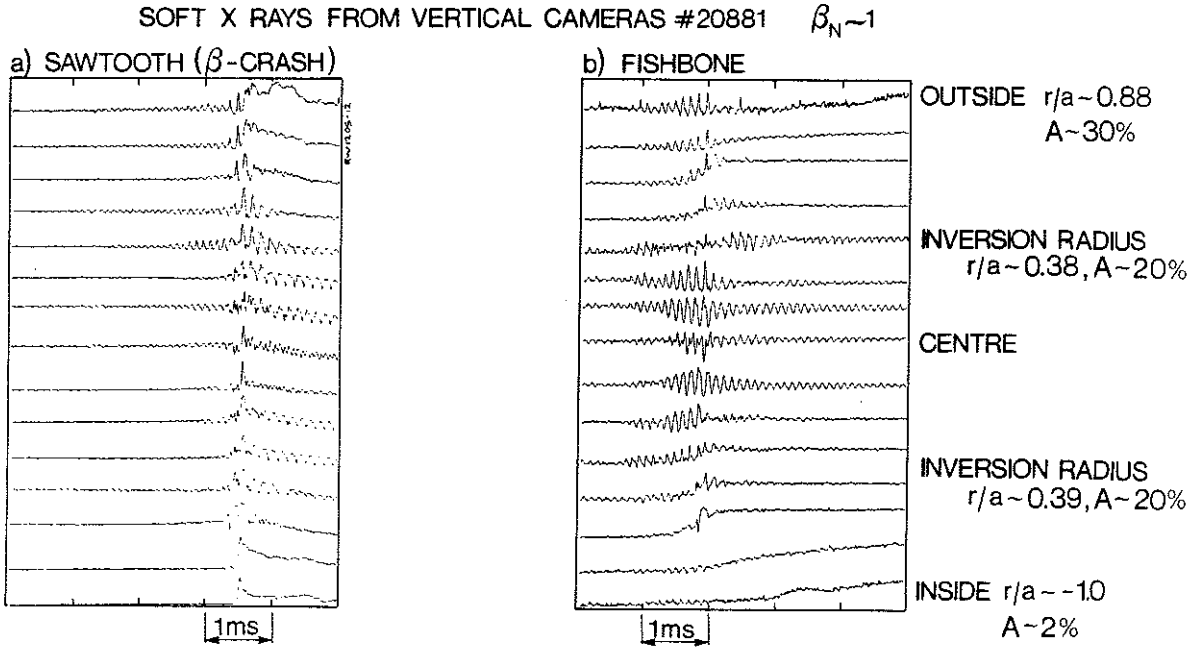

Figure 10 - Soft X-ray emission at different radial positions on the mid-plane, for a high beta sawtooth, on the left, and a fishbone burst, on the right.

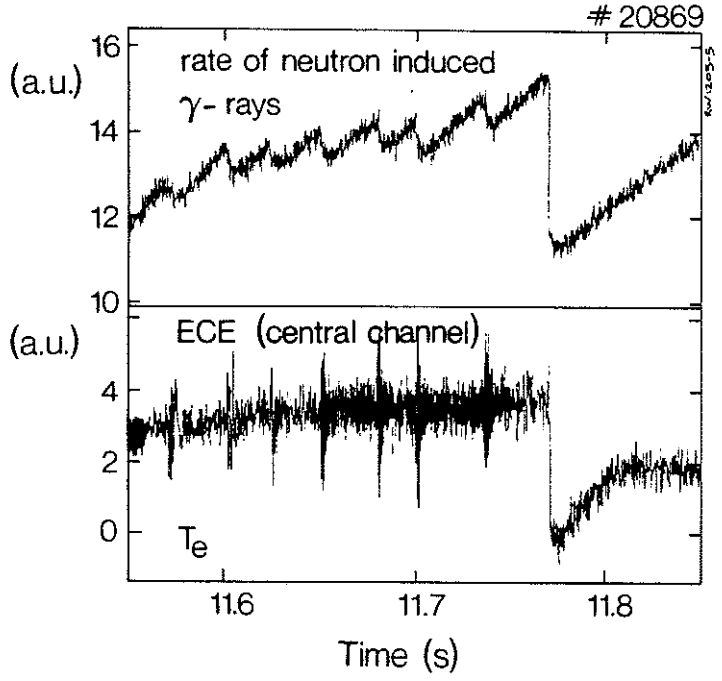

Figure 11 - Intensity of capture γ-rays exhibiting drops associated with fishbones observed in the ECE signal from the central region of the plasma. Through intercalibration with the fission chambers during the larger amplitude sawteeth, the drops in the global neutron emission are estimated to be about 9%.

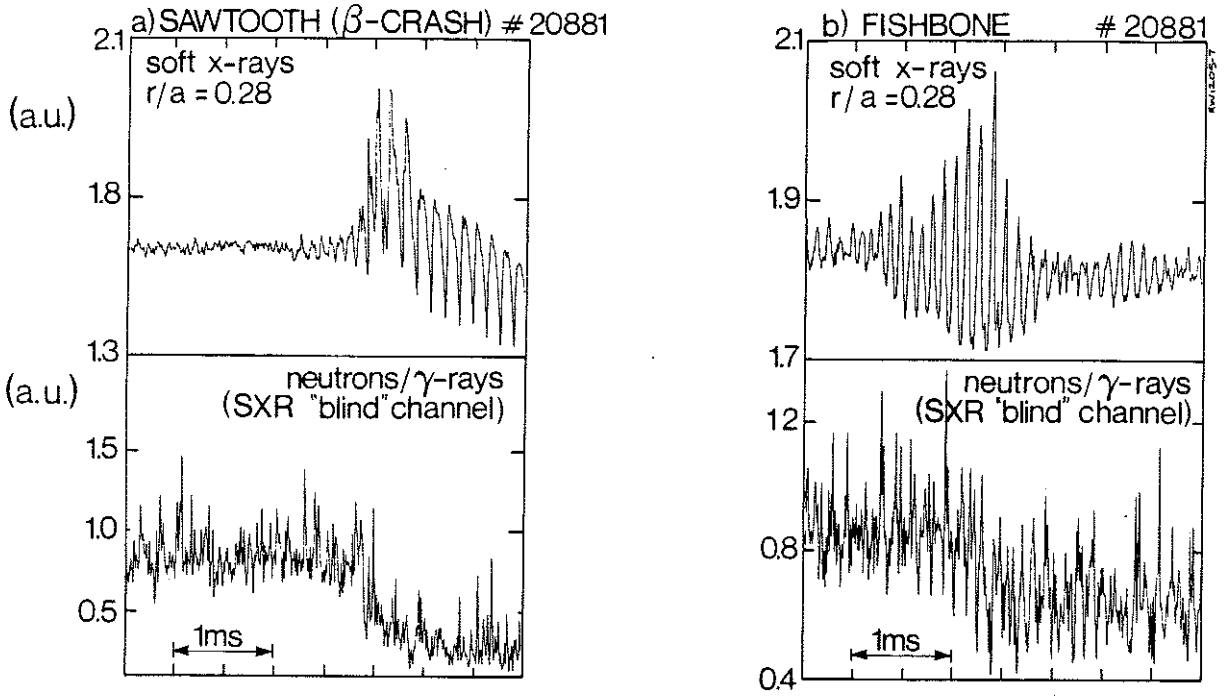

Figure 12 - Soft X-ray signals near to the sawtooth inversion radius for the high beta sawtooth and the fishbone burst of figure 10, and the corresponding signals from a silicon detector shielded with inconel, measuring mostly neutrons. Using a similar intercalibration technique an estimated drop of 19% in the neutron rate is obtained for the fishbone.

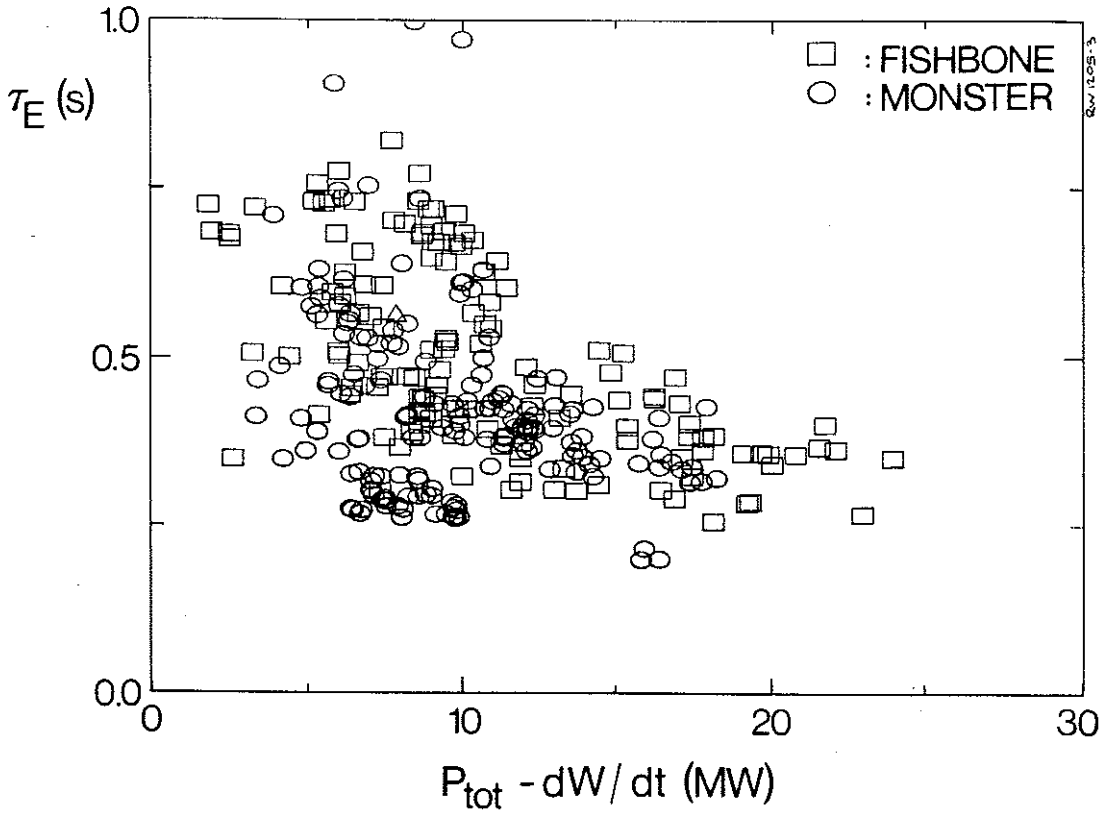

Figure 13 - Energy confinement time versus the total input power for observations of fishbone bursts and 'monster sawteeth', i.e. sawtooth-free periods.

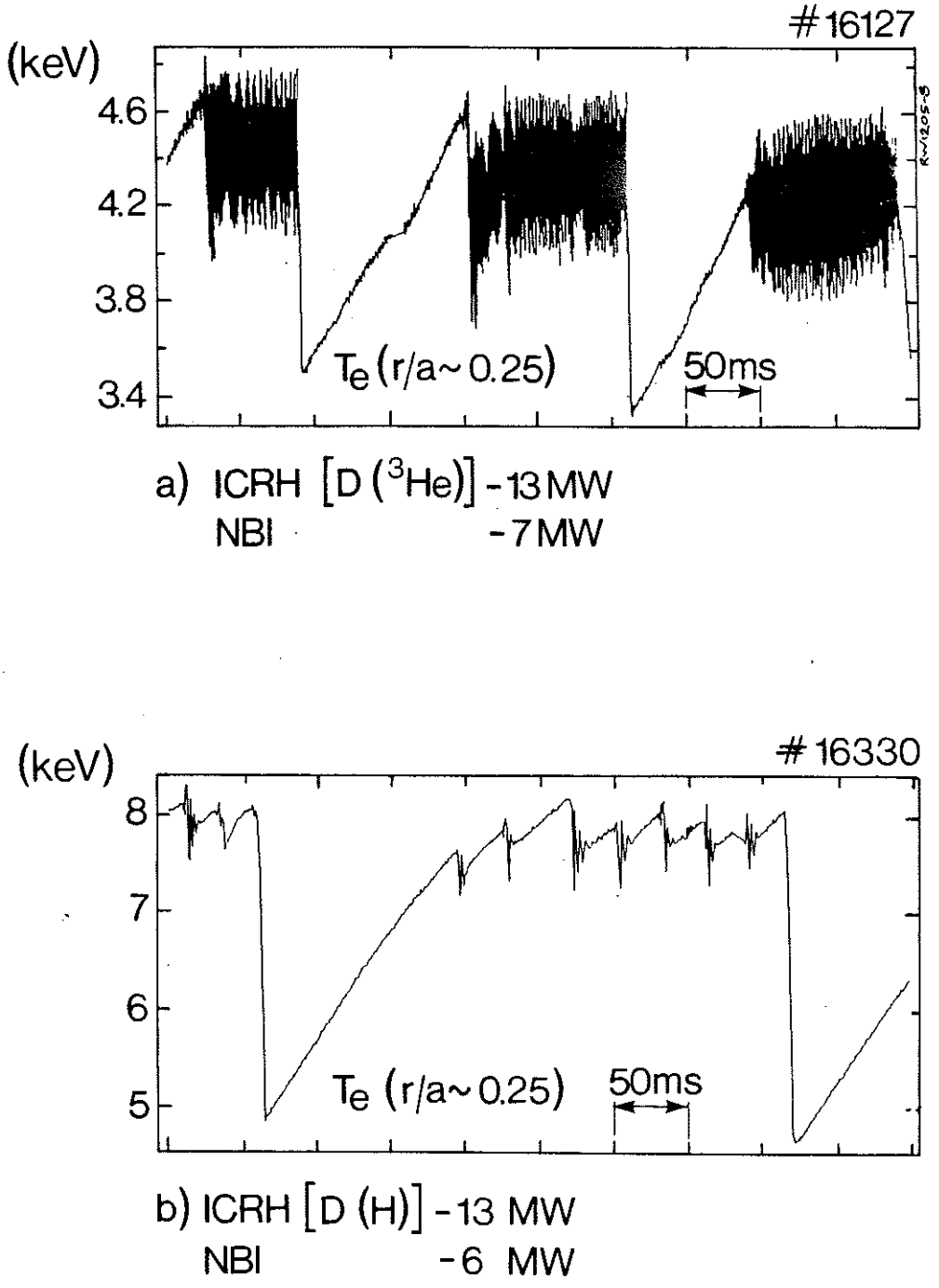

Figure 14 - Fishbone-like oscillations observed in the temperature signals of 5MA ICRH discharges heated with

a) ^{3}He minority gas and

b) H minority gas.

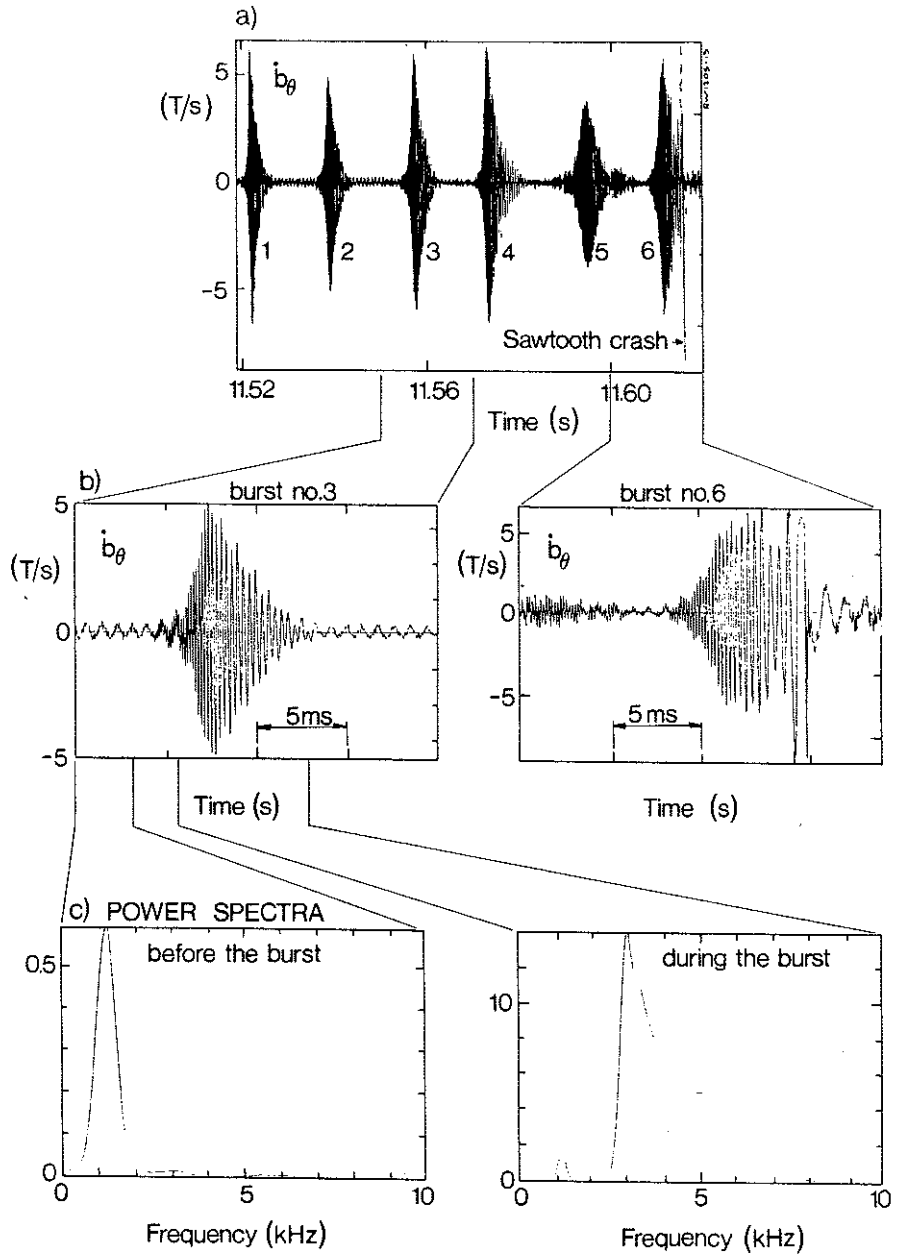

Figure 15 - (a) Magnetic signal (n=1 combination measured at 45° above the mid-plane on the lower field side) showing a sequency of fishbone bursts superimposed on a sawtooth ramp for a discharge with combined heating.

(b) An enlargement of (a) showing one of the bursts far from the sawtooth collapse and the burst immediately before the sawtooth collapse.

(c) Power spectra showing two oscillations with distinct frequencies present both in between and during the bursts. The slow oscillation has a constant amplitude and a constant frequency of 1.2kHz, comparable to the frequency of rotation of the plasma. (The frequency evolution of the fast oscillation during the burst is shown in Fig.6.) Both oscillations are present up to the sawtooth crash, which cuts short the burst duration. After the collapse postcursor oscillations are also observed.

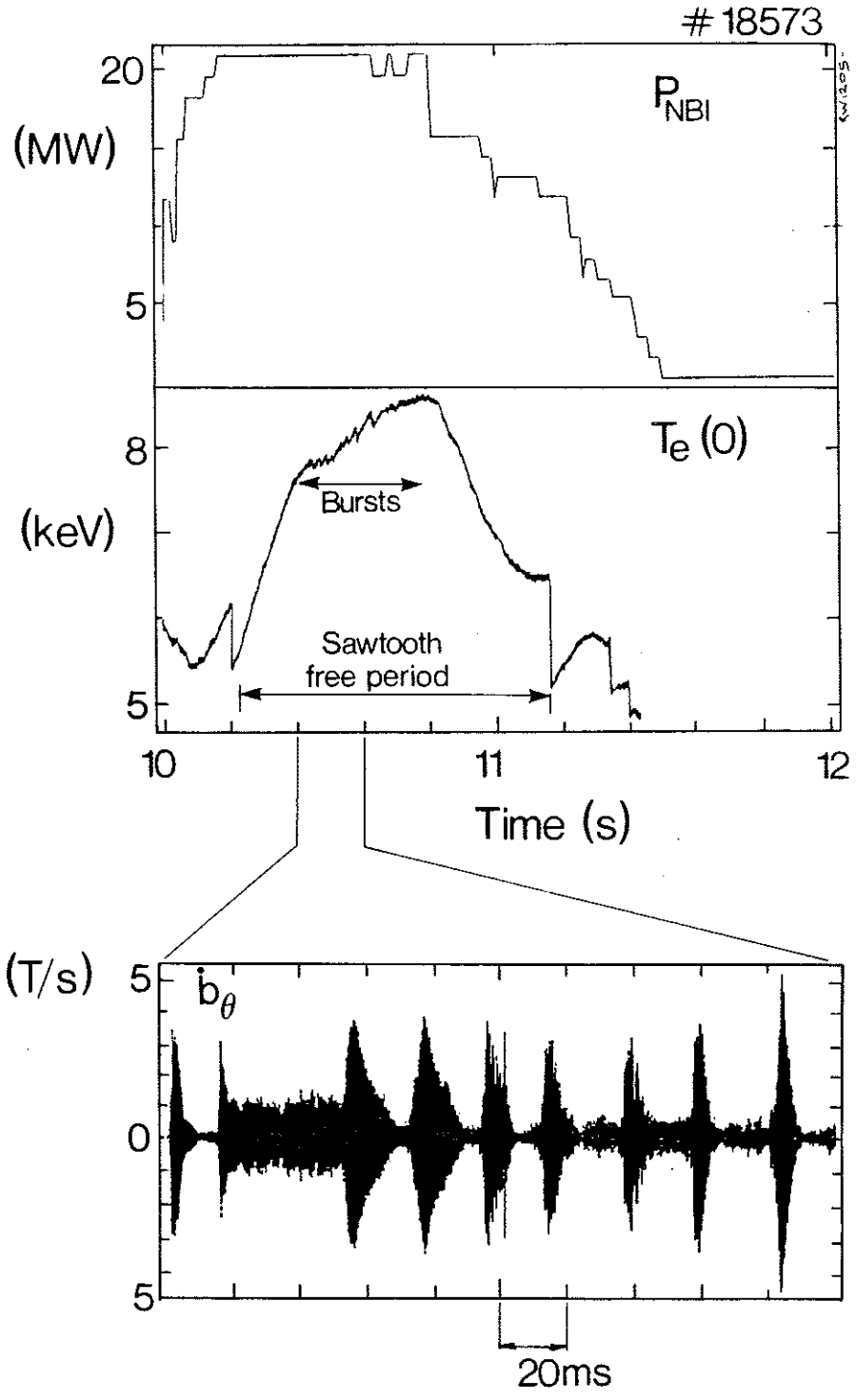

Figure 16 - Fishbones observed during a sawtooth-free period in a discharge heated with NBI only.

a) Plots of the total NBI power and the central temperature as function of time.

b) Magnetic signal (measured at 45° above the mid-plane on the lower field side) showing bursts associated to the small drops in temperature observed during the sawtooth free-period.

APPENDIX 1.

THE JET TEAM

JET Joint Undertaking, Abingdon, Oxon, OX14 3EA, U.K.

J.M.Adams[1], F.Alladio[4], H.Altmann, R.J.Anderson, G.Appruzzese, W.Bailey, B.Balet, D.V.Bartlett, L.R.Baylor[24], K.Behringer, A.C.Bell, P.Bertoldi, E.Bertolini, V.Bhatnagar, R.J.Bickerton, A.Boileau[3], T.Bonicelli, S.J.Booth, G.Bosia, M.Botman, D.Boyd[31], H.Brelen, H.Brinkschulte, M.Brusati, T.Budd, M.Bures, T.Businaro[4], H.Buttgereit, D.Cacaut, C.Caldwell-Nichols, D.J.Campbell, P.Card, J.Carwardine, G.Celentano, P.Chabert[27], C.D.Challis, A.Cheetham, J.Christiansen, C.Christodoulopoulos, P.Chuilon, R.Claesen, S.Clement[30], J.P.Coad, P.Colestock[6], S.Conroy[13], M.Cooke, S.Cooper, J.G.Cordey, W.Core, S.Corti, A.E.Costley, G.Cottrell, M.Cox[7], P.Cripwell[13], F.Crisanti[4], D.Cross, H.de Blank[16], J.de Haas[16], L.de Kock, E.Deksnis, G.B.Denne, G.Deschamps, G.Devillars, K.J.Dietz, J.Dobbing, S.E.Dorling, P.G.Doyle, D.F.Düchs, H.Duquenoy, A.Edwards, J.Ehrenberg[14], T.Elevant[12], W.Engelhardt, S.K.Erents[7], L.G.Eriksonn[5], M.Evrard[2], H.Falter, D.Flory, M.Forrest[7], C.Froger, K.Fullard, M.Gadeberg[11], A.Galetsas, R.Galvao[8], A.Gibson, R.D.Gill, A.Gondhalekar, C.Gordon, G.Gorini, C.Gormezano, N.A.Gottardi, C.Gowers, B.J.Green, F.S.Griph, M.Gryzinski[26], R.Haange, G.Hammett[6], W.Han[9], C.J.Hancock, P.J.Harbour, N.C.Hawkes[7], P.Haynes[7], T.Hellsten, J.L.Hemmerich, R.Hemsworth, R.F.Herzog, K.Hirsch[14], J.Hoekzema, W.A.Houlberg[24], J.How, M.Huart, A.Hubbard, T.P.Hughes[32], M.Hugon, M.Huguet, J.Jacquinot, O.N.Jarvis, T.C.Jernigan[24], E.Joffrin, E.M.Jones, L.P.D.F.Jones, T.T.C.Jones, J.Källne, A.Kaye, B.E.Keen, M.Keilhacker, G.J.Kelly, A.Khare[15], S.Knowlton, A.Konstantellos, M.Kovanen[21], P.Kupschus, P.Lallia, J.R.Last, L.Lauro-Taroni, M.Laux[33], K.Lawson[7], E.Lazzaro, M.Lennholm, X.Litaudon, P.Lomas, M.Lorentz-Gottardi[2], C.Lowry, G.Magyar, D.Maisonnier, M.Malacarne, V.Marchese, P.Massmann, L.McCarthy[28], G.McCracken[7], P.Mendonca, P.Meriguet, P.Micozzi[4], S.F.Mills, P.Millward, S.L.Milora[24], A.Moissonnier, P.L.Mondino, D.Moreau[17], P.Morgan, H.Morsi[14], G.Murphy, M.F.Nave, M.Newman, L.Nickesson, P.Nielsen, P.Noll, W.Obert, D.O'Brien, J.O'Rourke, M.G.Pacco-Düchs, M.Pain, S.Papastergiou, D.Pasini[20], M.Paume[27], N.Peacock[7], D.Pearson[13], F.Pegoraro, M.Pick, S.Pitcher[7], J.Plancoulaine, J-P.Poffé, F.Porcelli, R.Prentice, T.Raimondi, J.Ramette[17], J.M.Rax[27], C.Raymond, P-H.Rebut, J.Removille, F.Rimini, D.Robinson[7], A.Rolfe, R.T.Ross, L.Rossi, G.Rupprecht[14], R.Rushton, P.Rutter, H.C.Sack, G.Sadler, N.Salmon[13], H.Salzmann[14], A.Santagiustina, D.Schissel[25], P.H.Schild, M.Schmid, G.Schmidt[6], R.L.Shaw, A.Sibley, R.Simonini, J.Sips[16], P.Smeulders, J.Snipes, S.Sommers, L.Sonnerup, K.Sonnenberg, M.Stamp, P.Stangeby[19], D.Start, C.A.Steed, D.Stork, P.E.Stott, T.E.Stringer, D.Stubberfield, T.Sugie[18], D.Summers, H.Summers[20], J.Taboda-Duarte[22], J.Tagle[30], H.Tamnen, A.Tanga, A.Taroni, C.Tebaldi[23], A.Tesini, P.R.Thomas, E.Thompson, K.Thomsen[11], P.Trevalion, M.Tschudin, B.Tubbing, K.Uchino[29], E.Usselmann, H.van der Beken, M.von Hellermann, T.Wade, C.Walker, B.A.Wallander, M.Walravens, K.Walter, D.Ward, M.L.Watkins, J.Wesson, D.H.Wheeler, J.Wilks, U.Willen[12], D.Wilson, T.Winkel, C.Woodward, M.Wykes, I.D.Young, L.Zannelli, M.Zarnstorff[6], D.Zasche[14], J.W.Zwart.

PERMANENT ADDRESS

1. UKAEA, Harwell, Oxon. UK.
2. EUR-EB Association, LPP-ERM/KMS, B-1040 Brussels, Belgium.
3. Institute National des Récherches Scientifique, Quebec, Canada.
4. ENEA-CENTRO Di Frascati, I-00044 Frascati, Roma, Italy.
5. Chalmers University of Technology, Göteborg, Sweden.
6. Princeton Plasma Physics Laboratory, New Jersey, USA.
7. UKAEA Culham Laboratory, Abingdon, Oxon. UK.
8. Plasma Physics Laboratory, Space Research Institute, Sao José dos Campos, Brazil.
9. Institute of Mathematics, University of Oxford, UK.
10. CRPP/EPFL, 21 Avenue des Bains, CH-1007 Lausanne, Switzerland.
11. Risø National Laboratory, DK-4000 Roskilde, Denmark.
12. Swedish Energy Research Commission, S-10072 Stockholm, Sweden.
13. Imperial College of Science and Technology, University of London, UK.
14. Max Planck Institut für Plasmaphysik, D-8046 Garching bei München, FRG.
15. Institute for Plasma Research, Gandhinagar Bhat Gujat, India.
16. FOM Instituut voor Plasmafysica, 3430 Be Nieuwegein, The Netherlands.
17. Commissiariat à L'Energie Atomique, F-92260 Fontenay-aux-Roses, France.
18. JAERI, Tokai Research Establishment, Tokai-Mura, Naka-Gun, Japan.
19. Institute for Aerospace Studies, University of Toronto, Downsview, Ontario, Canada.
20. University of Strathclyde, Glasgow, G4 ONG, U.K.
21. Nuclear Engineering Laboratory, Lapeenranta University, Finland.
22. JNICT, Lisboa, Portugal.
23. Department of Mathematics, Univeristy of Bologna, Italy.
24. Oak Ridge National Laboratory, Oak Ridge, Tenn., USA.
25. G.A. Technologies, San Diego, California, USA.
26. Institute for Nuclear Studies, Swierk, Poland.
27. Commissiariat à l'Energie Atomique, Cadarache, France.
28. School of Physical Sciences, Flinders University of South Australia, South Australia SO42.
29. Kyushi University, Kasagu Fukuoka, Japan.
30. Centro de Investigaciones Energeticas Medioambientales y Techalogicas, Spain.
31. University of Maryland, College Park, Maryland, USA.
32. University of Essex, Colchester, UK.
33. Akademie de Wissenschaften, Berlin, DDR.

CR 88.49.1A